electronic reprint

Journal of
Applied Crystallography
ISSN 0021-8898

Twinning in $La_{0.95}Sr_{0.05}Ga_{0.9}Mg_{0.1}O_{2.92}$ crystal studied by white-beam (Laue) X-ray microdiffraction

D. I. Savytskii, D. M. Trots, L. O. Vasylechko, N. Tamura and M. Berkowski

Journal of
Applied Crystallography
ISSN 0021-8898

Received 24 February 2003
Accepted 26 June 2003

Twinning in $La_{0.95}Sr_{0.05}Ga_{0.9}Mg_{0.1}O_{2.92}$ crystal studied by white-beam (Laue) X-ray microdiffraction

D. I. Savytskii,[a]* D. M. Trots,[a] L. O. Vasylechko,[a] N. Tamura[b] and M. Berkowski[c]

[a]Lviv Polytechnic National University, 12 Bandera St., 79013, Lviv, Ukraine, [b]Lawrence Berkeley National Laboratory, 1 Cyclotron Road, Berkeley, CA 94720, USA, and [c]Institute of Physics, Polish Academy of Sciences, Al. Lotnikow 32/46, 02-668, Warsaw, Poland. Correspondence e-mail: crystal@polynet.lviv.ua

The investigation of twin structure in $La_{0.95}Sr_{0.05}Ga_{0.9}Mg_{0.1}O_{2.92}$ perovskite-type crystals has been undertaken using the technique of white-beam X-ray microdiffraction. The sample shows definite twinning which is reflected in the Laue patterns as apparent splitting of the peaks. Reflections from the different domains were indexed separately. Positional shifts of twin domain spots with respect to the reference matrix spot, arising from the mutual misorientation of diffraction vectors, were measured on Laue patterns and compared with calculated values in order to solve the twin laws in this system. The dominant twin operations were found to be $(12\bar{1})$ and $(10\bar{1})$ mirror reflections.

1. Introduction

Twin domains and their boundaries are the dominant microstructural features in many materials. It has been shown theoretically and experimentally that diffusion of dopant ions or vacancies occurs at an enhanced rate within twin domain walls (Aird & Salje, 1998; Lee *et al.*, 2003). Furthermore, impurities may be pinned in the wall or in its close vicinity (Bartels *et al.*, 2003). The fact that walls and bulk material show different dielectric transport and diffusion rates could be very useful to explain the high ionic conductivity in heavily twinned doped lanthanum gallates, which are of interest as potential electrolytes in solid oxide fuel cells (Feng & Goodenough, 1994; Ishihara *et al.*, 1995).

Efforts to understand the influence of domain structure on certain physical properties were mainly focused on computer modeling, while experimental data of comparable quality remain difficult to obtain. Most of the publications on this subject rely on the direct visualization of domains by transmission electron microscopy (Tendeloo *et al.*, 1990; Putnis & Salje, 1994; Zhu *et al.*, 1990). The disadvantage of this technique is that it is destructive, requires careful sample preparation and is restricted to very small areas of the sample. Recently, white-beam X-ray diffraction topography using synchrotron radiation sources turned out to be a simple, fast and efficient imaging technique for the investigation of domain structures (Yao *et al.*, 1991; Huang *et al.*, 1996; Medrano *et al.*, 1999; Chikaura *et al.*, 2001). Information regarding twin laws and twin distribution can be simultaneously obtained from a large area of the specimen. The disadvantage of this technique is its poor spatial resolution and the possible overlapping of images coming from different reflections.

In the present paper, we report the non-destructive investigation of twins in $La_{0.95}Sr_{0.05}Ga_{0.9}Mg_{0.1}O_{2.92}$ (LSGM-05) perovskite-type crystals using the technique of white-beam (polychromatic) X-ray microdiffraction (also called the X-ray microdiffraction Laue technique) (Tamura *et al.*, 2002). This tool does not have the disadvantages of the above-mentioned techniques and can be used for *in situ* measurements under a variety of different experimental conditions. It can, in particular, be used for characterization (determination of twin laws, misorientation of domains and domain wall orientations) of twin structure both in small crystals and local areas of large samples.

2. Experimental details

LSGM-05 single crystals with diameters of 15 mm and lengths of 25–30 mm were grown from the melt in Ar atmosphere using the Czochralski technique.

Laue experiments were carried out on the X-ray microdiffraction end-station (7.3.3.) at the Advanced Light Source. The instrument is capable of delivering a focused X-ray white beam (5–14 keV) with a size less than 1 μm by using a pair of elliptically bent mirrors in a Kirkpatrick–Baez configuration. Diffraction data were collected in reflection mode using a large-area Bruker SMART 6000 CCD camera mounted on a vertical slide. The CCD dimensions are 93.865 × 93.865 mm and we used the 1024 × 1024 pixels binning mode. The sample surface was set to be at 45° relative to the incoming beam. The distance from the CCD to the sample was determined to be 36.0 mm. The CCD center was determined to be at 496.8, 564.2 pixels. The sample surface was approximately parallel to the (103), (301) or (222) planes depending on the domain considered.

Table 1
Twin structure parameters of LSGM crystal.

Twin state pair	Symmetry elements which connect the states	Wall type	Wall orientation in perovskite and orthorhombic representation		Tensor $\boldsymbol{T}_t$ of the relationship for twin pair	Tensor $\boldsymbol{Tobs}_i$ of the relationship	Experimental domain pair
D_1–D_2	$\boldsymbol{m}_x$ $\boldsymbol{2}_y$ $\bar{4}_z$ 4_z^3 4_z $4_z^{\bar{3}}$ $\boldsymbol{m}_y$ $\boldsymbol{2}_x$	W'_{12}	$(1\,0\,0)_p$	$(1\,0\,1)$	$\begin{pmatrix} -0.007 & 0 & -0.993 \\ 0 & -1 & 0 \\ -1.007 & 0 & 0.007 \end{pmatrix}$		
		W''_{12}	$(0\,1\,0)_p$	$(1\,0\,\bar{1})$	$\begin{pmatrix} -0.007 & 0 & 0.993 \\ 0 & -1 & 0 \\ 1.007 & 0 & 0.007 \end{pmatrix}$	$\begin{pmatrix} -0.018 & -0.006 & 0.984 \\ -0.001 & -1 & -0.006 \\ 1.007 & -0.001 & 0.005 \end{pmatrix}$	*A*–*C*
D_1–D_3	$\boldsymbol{m}_{xz}$ $\bar{4}_y$ $\bar{3}_{-x-yz}$ $\bar{3}_{x-y-z}$ 4_y 3_{-x-yz} 3_{x-y-z} $\boldsymbol{2}_{xz}$	W_{13}	$(1\,0\,1)_p$	$(1\,2\,1)$	$\begin{pmatrix} 0.497 & -0.501 & -0.496 \\ -1.006 & -0.001 & -0.992 \\ -0.503 & -0.501 & 0.504 \end{pmatrix}$		
		S_{13}	$(1\,5.31\,\bar{1})_p$	$(2.15\,1\,\overline{3.15})$	$\begin{pmatrix} -0.503 & 0.497 & 0.497 \\ 0.999 & -0.001 & 0.999 \\ 0.504 & 0.504 & -0.496 \end{pmatrix}$		
D_1–D_4	$\boldsymbol{m}_{-xz}$ $\bar{4}_y^3$ $\bar{3}_{xyz}$ $\bar{3}_{-xy-z}$ 4_y^3 3_{xyz} 3_{-xy-z} $\boldsymbol{2}_{-xz}$	W_{14}	$(1\,0\,\bar{1})_p$	$(1\,\bar{2}\,1)$	$\begin{pmatrix} 0.497 & 0.501 & -0.496 \\ 1.006 & -0.001 & 0.992 \\ -0.503 & 0.501 & 0.504 \end{pmatrix}$		
		S_{14}	$(1\,5.31\,1)_p$	$(\overline{2.15}\,1\,3.15)$	$\begin{pmatrix} -0.503 & -0.497 & 0.497 \\ -0.999 & -0.001 & -0.999 \\ 0.504 & -0.504 & -0.496 \end{pmatrix}$		
D_1–D_5	$\boldsymbol{m}_{yz}$ $\bar{3}^2_{-x-yz}$ $\bar{4}_x^3$ $\bar{3}^2_{-xy-z}$ 4_x^3 3^2_{-x-yz} 3^2_{-xy-z} $\boldsymbol{2}_{yz}$	W_{15}	$(0\,1\,1)_p$	$(\bar{1}\,2\,1)$	$\begin{pmatrix} 0.497 & 0.501 & 0.496 \\ 1.006 & -0.001 & -0.992 \\ 0.503 & -0.501 & 0.504 \end{pmatrix}$	$\begin{pmatrix} 0.490 & 0.497 & 0.495 \\ 1.016 & 0.008 & -0.985 \\ 0.500 & -0.503 & 0.494 \end{pmatrix}$	*A*–*E*
		S_{15}	$(5.31\,1\,\bar{1})_p$	$(2.15\,\bar{1}\,3.15)$	$\begin{pmatrix} -0.503 & -0.497 & -0.497 \\ -0.999 & -0.001 & 0.999 \\ -0.504 & 0.504 & -0.496 \end{pmatrix}$		
D_1–D_6	$\boldsymbol{m}_{-yz}$ $\bar{4}_x$ $\bar{3}^2_{xyz}$ $\bar{3}^2_{x-y-z}$ 4_x 3^2_{xyz} 3^2_{x-y-z} $\boldsymbol{2}_{-yz}$	W_{16}	$(0\,1\,\bar{1})_p$	$(1\,2\,\bar{1})$	$\begin{pmatrix} 0.497 & -0.501 & 0.496 \\ -1.006 & -0.001 & 0.992 \\ 0.503 & 0.501 & 0.504 \end{pmatrix}$	$\begin{pmatrix} 0.493 & -0.505 & 0.484 \\ -1.014 & -0.009 & 0.987 \\ 0.499 & 0.497 & 0.503 \end{pmatrix}$	*A*–*B*
		S_{16}	$(5.31\,1\,1)_p$	$(2.15\,1\,3.15)$	$\begin{pmatrix} -0.503 & 0.497 & -0.497 \\ 0.999 & -0.001 & -0.999 \\ -0.504 & -0.504 & -0.496 \end{pmatrix}$		

We used custom software developed at the ALS (*X-MAS*, *X-ray Microdiffraction Analysis Software*) to analyze the collected white-beam (Laue) diffraction patterns. The reflection positions in the patterns were accurately determined with subpixel resolution by fitting their two-dimensional peak profiles with a two-dimensional Pearson VII function. From the peak positions and known lattice parameters of the crystal, the patterns were indexed with *h*,*k*,*l* Miller indices, from which orientation matrices of the illuminated area of the crystals were obtained.

3. Theoretical consideration

3.1. Crystallographic characterization

$La_{0.95}Sr_{0.05}Ga_{0.9}Mg_{0.1}O_{2.92}$ has a perovskite-type structure, which experiences a few phase transitions. At high temperature, LSGM-05 undergoes three phase transitions: orthorhombic to monoclinic (*Imma* $\rightarrow$ *I*2/*a*) at 520–570 K, monoclinic to trigonal (*I*2/*a* $\rightarrow$ *R*$\bar{3}$*c*) at 720 K, and trigonal to trigonal (*R*3*c* $\rightarrow$ *R*$\bar{3}$*c*) at *ca* 870 K (Vasylechko *et al.*, 2003). The prototype phase of the crystal is the cubic perovskite structure, which belongs to the point group *m*3*m* and the space group *Pm*3*m*. From an extrapolation of the thermal behaviour of perovskite-type cell parameters, we conclude that $La_{0.95}Sr_{0.05}Ga_{0.9}Mg_{0.1}O_{2.92}$ undergoes a phase transition to the cubic phase at a temperature which is close to the melting point of the compound. At room temperature the structure is orthorhombic with the point group *mmm* and the space group *Imma* (Vasylechko *et al.*, 2003).

The symmetry of the room-temperature phase is a subgroup of the symmetry of the cubic prototype phase. This phase transition is thus of the paraelastic ferroelastic type, and is

Table 2
Twin states of LSGM with the corresponding unique diad (stretching axis) and spontaneous strain tensors.

$\tau = (1/2)\mathrm{tg}(\pi/2 - \gamma_p)$; $\beta = (1/3)(a_p - a_0)/a_0 - (1/3)(c_p - a_0)/a_0$; $a_0 = (abc/4)^{1/3}$.

	Twin state					
	D_1	D_2	D_3	D_4	D_5	D_6
Stretching axis	$[110]_p$	$[\bar{1}10]_p$	$[101]_p$	$[10\bar{1}]_p$	$[011]_p$	$[0\bar{1}1]_p$
Spontaneous strain tensor	$\begin{pmatrix} \beta & \tau & 0 \\ \tau & \beta & 0 \\ 0 & 0 & -2\beta \end{pmatrix}$	$\begin{pmatrix} \beta & -\tau & 0 \\ -\tau & \beta & 0 \\ 0 & 0 & -2\beta \end{pmatrix}$	$\begin{pmatrix} -2\beta & 0 & 0 \\ 0 & \beta & -\tau \\ 0 & -\tau & \beta \end{pmatrix}$	$\begin{pmatrix} -2\beta & 0 & 0 \\ 0 & \beta & \tau \\ 0 & \tau & \beta \end{pmatrix}$	$\begin{pmatrix} \beta & 0 & -\tau \\ 0 & -2\beta & 0 \\ -\tau & 0 & \beta \end{pmatrix}$	$\begin{pmatrix} \beta & 0 & \tau \\ 0 & -2\beta & 0 \\ \tau & 0 & \beta \end{pmatrix}$

labeled as Aizu species *m*3*mFmmm* (Aizu, 1970). The unit-cell axes of the *Imma* phase are given in terms of the pseudo-perovskite cell axes by the matrix

$$\begin{pmatrix} \mathbf{a} \\ \mathbf{b} \\ \mathbf{c} \end{pmatrix} = \begin{pmatrix} 1 & -1 & 0 \\ 0 & 0 & 2 \\ 1 & 1 & 0 \end{pmatrix} \times \begin{pmatrix} \mathbf{a}_p \\ \mathbf{b}_p \\ \mathbf{c}_p \end{pmatrix} \qquad (1)$$

and origin choice $(0,0,0) = (-0.5,0.5,0)_p$ (Fig. 1).

The orthorhombic *Imma* cell has lattice parameters a = 5.4990, b = 7.7942, c = 5.5381 Å (Vasylechko *et al.*, 2003). The pseudocubic subcell, which conveniently relates the cubic prototype unit cell to unit cells of the different high-temperature phases, is monoclinic with lattice parameters $a_p = b_p = [(a^2 + c^2)/4]^{1/2}$ = 3.9022 Å, $c_p = b/2$ = 3.8971 Å, $\gamma_p = 2\,\mathrm{arctg}(a/c)$ = 89.594°, where a, b and c are the lattice parameters of the orthorhombic room-temperature phase. The subscript p denotes a pseudo-perovskite cell.

3.2. Parameters of twin structure

A fundamental approach to understand the possible domain variants formed during a phase transition due to the symmetry change is to use group theory (Aizu, 1970; Janovec, 1972). Symmetry breaking at the phase transition gives rise to energetically equivalent domain states in the room-temperature phase, related to one another by symmetry elements, which have been lost with respect to the prototype symmetry. The domain states include twin (orientation) states, which result from the loss of point-group symmetry, as well as anti-phase domains arising from the loss of translational symmetry. Only twin domain states are macroscopically distinguishable by the X-ray Laue diffraction technique. Therefore, we will only consider the symmetry breaking of the point group at the phase transition. The number of twin states is six, which is the group–subgroup index of the point group *mmm* (order 8) (Fig. 1*b*) in the point group *m*3*m* (order 48). From an analysis of the coset decomposition of the *m*3*m* supergroup with respect to its *mmm* subgroup, we found symmetry elements (F) which connect the corresponding domain pairs (Table 1). As is seen from Table 1, a diad axis 2 and a mirror plane m, which is perpendicular to this axis, are F operations between the domain states D_1 and D_i (i = 2 . . . 6). These symmetry elements are in bold in Table 1. In these cases according to Sapriel (1975) the mirror plane m is one of the permissible walls between a D_1 and D_i domain pair and another wall contains the diad axis 2. For example, such symmetry elements between D_1 and D_5 domains are 2_{yz} and m_{yz}. Correspondingly, the plane $(011)_p$ or $(\bar{1}21)$ in orthorhombic representation is one of the expected walls between the D_1 and D_5 domain pair and the second domain wall contains the $[011]_p$ crystallographic direction ($[11\bar{1}]$ in orthorhombic setting).

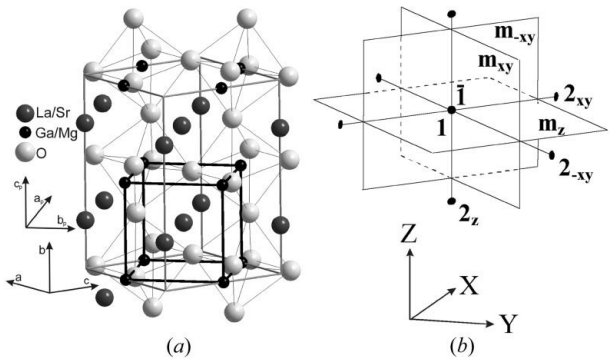

Figure 1
Orthorhombic and perovskite-type monoclinic cells (*a*) and symmetry elements of the point group *mmm* (*b*).

The number of twin states and the orientation of domain walls can also be explained as follows. The room-temperature orthorhombic structure is considered as a perovskite cubic cell slightly stretched along the face diagonal $[110]_p$. The stretching along the other five equivalent face diagonals of the cube results in corresponding equivalent distortions of the cell. The spatial orientation of these states in an orthorhombic ferroelastic phase is shown in Fig. 2. The spontaneous strain of the twin states in the room-temperature phase determines the possible orientations of the domain walls and can be described by the six strain tensors given in Table 2. The strain for every twin domain states is indicated in Fig. 2. According to Sapriel (1975) allowed twin walls can be found by the condition

$$\sum_{j,k}^{3} (e_{jk,1} - e_{jk,i}) x_j x_k = 0, \qquad (2)$$

where $e_{jk}(D_1, D_i)$ are the strain tensor elements of the adjacent domains D_1 and D_i, respectively. In our case the solutions are planes with ten different orientations. Table 1 lists the allowed domains walls between each pair of domain states D_1 and D_i. These solutions are either mirror planes (marked by symbol W in Table 1) or walls (S), which contain the twofold axes of a paraelastic perovskite cube that correspond to the results of a group theory method.

As seen from Table 1, the twin state D_2 is connected with the state D_1 by mirror reflection with respect to $(100)_p$ or $(010)_p$ and 180° rotation around $[010]_p$ or $[100]_p$. Domain walls are (101) (Fig. 3*a*) or $(10\bar{1})$ planes, respectively. The twin orientation states $D_3 \ldots D_6$ are connected with D_1 *via* mirror reflection of a certain plane from the $(101)_p$ or $(011)_p$ set or *via* rotation around the twofold axes from the $\langle 101\rangle_p$ or $\langle 011\rangle_p$ ($\langle 111\rangle$) family. For reflection twins, the interface boundaries between the matrix and the twin crystal parts are the (121) set of planes (*W* type) (Fig. 3*b*), whereas for axial twins they have non-integer Miller indices (*S* type) (Fig. 3*c*). The orientation of these walls was determined by a spontaneous strain method (Sapriel, 1975).

The above theoretical analysis of the twin structure of LSGM-05 allows one to correlate each twin law with a matrix connected to the orthorhombic or pseudo-perovskite basis vectors of neighboring domains. Using the twin models shown in Fig. 3 and an analytical geometry approach, the relationships of the orthorhombic basis vectors were obtained for all possible domain pairs. The orthorhombic basis vectors $\mathbf{a}^t$, $\mathbf{b}^t$, $\mathbf{c}^t$ of the $D_2 \ldots D_6$ domains ($t = 1 \ldots 10$) were expressed by means of the basis vectors $\mathbf{a}^0$, $\mathbf{b}^0$, $\mathbf{c}^0$ of the D_1 domain:

$$\begin{pmatrix} \mathbf{a}^t \\ \mathbf{b}^t \\ \mathbf{c}^t \end{pmatrix} = \boldsymbol{T}_t \times \begin{pmatrix} \mathbf{a}^0 \\ \mathbf{b}^0 \\ \mathbf{c}^0 \end{pmatrix}, \qquad (3)$$

where $\boldsymbol{T}_t$ are second-rank tensors. The calculated tensors $\boldsymbol{T}_t$ of the relationship for all permitted twin laws are shown in Table 1.

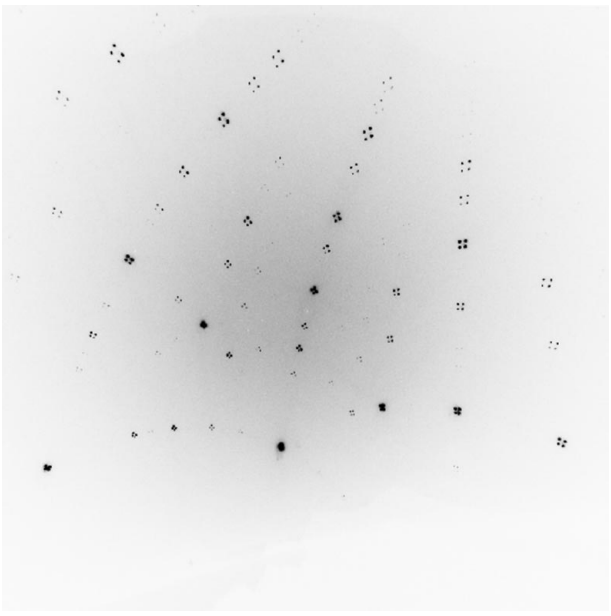

Figure 4
Laue pattern of sample LSGM-05 at room temperature.

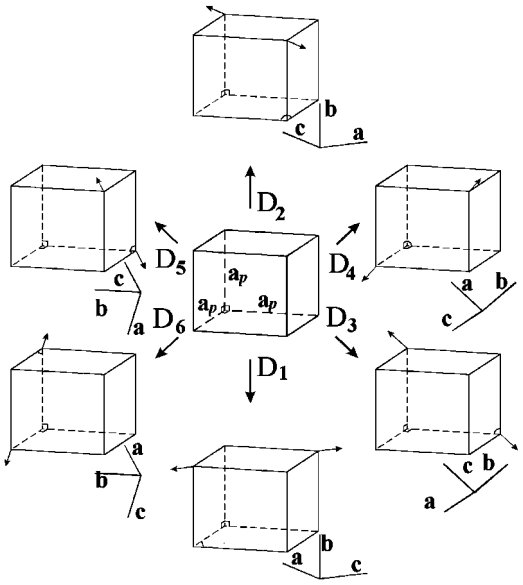

Figure 2
Spatial orientation of six domain states in LSGM crystal and appropriate deformations of the perovskite cell.

4. Experimental results

The X-ray microdiffraction Laue technique enables the identification and characterization of twin structures of the crystal. Using the broad wavelength range provided by synchrotron radiation, twin domains in crystals can be identified owing to different orientations, *i.e.* the differently oriented domains select different wavelengths for diffraction and give spots that are shifted with respect to one another

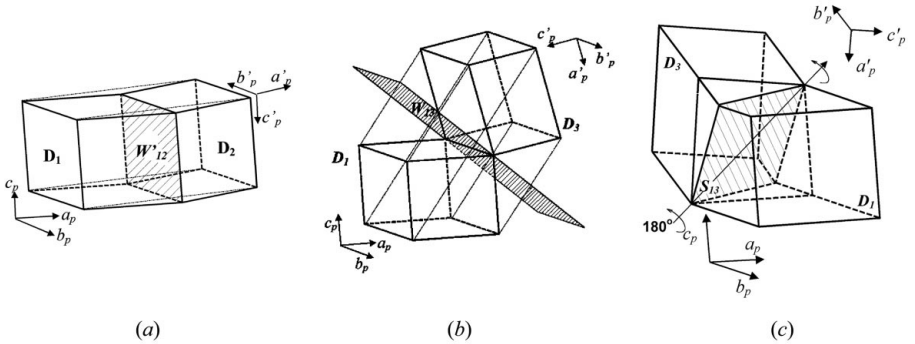

Figure 3
Scheme of twinning (*a*) relative to mirror reflection plane W'_{12} (101) $[(100)_p]$ and 180° rotation around $[10\bar{1}]$ $([010]_p)$ (perovskite-type cells of D_1 and D_2 orientation states), (*b*) relative to mirror reflection plane W_{13} (121) $[(101)_p]$ (perovskite-type cells of D_1 and D_3 orientation states), (*c*) in the case of a 180° turn around the [111] $([101]_p)$ (perovskite-type cells of D_1 and D_3 orientation states separated by S_{13} wall).

Table 3
The calculated orientation matrices from experimental data.

	Experimental twin state			
	A	*B*	*C*	*E*
Orientation matrix	$\begin{pmatrix} -4.453 & -2.825 & 1.558 \\ -1.693 & -1.451 & -7.469 \\ -3.108 & 4.638 & -0.217 \end{pmatrix}$	$\begin{pmatrix} 2.844 & -1.586 & -4.431 \\ -1.463 & -7.457 & 1.730 \\ 4.624 & -0.202 & 3.041 \end{pmatrix}$	$\begin{pmatrix} -2.971 & 4.623 & -0.200 \\ 1.715 & 1.423 & 7.469 \\ -4.498 & -2.823 & 1.571 \end{pmatrix}$	$\begin{pmatrix} -4.561 & 0.188 & -3.066 \\ 1.477 & 7.452 & -1.740 \\ -2.910 & 1.611 & 4.428 \end{pmatrix}$

depending on the particular reflection in the Laue pattern. From the experimental Laue pattern, an orientation matrix for each separate domain can be calculated as long as the lattice parameters of the crystal are known. In this way every spot splitting of the pattern could be indexed. Then these orientation matrices can be used to reveal the orientation relationships and therefore the twin laws between the domains could be established.

Fig. 4 shows a characteristic Laue pattern obtained at room temperature from the LSGM-05 sample. The sample shows definite twinning, which is reflected in the Laue pattern as apparent splitting of the peaks into four reflections. Reflections from the four different domains were indexed separately. Indexing for domains *A*, *B*, *C* and *E* is shown in Fig. 5. The patterns were indexed in the orthorhombic symmetry with lattice parameters a = 5.449, b = 7.794, c = 5.538 Å. The orientation matrices $\boldsymbol{M}_i$ (i = *A*, *B*, *C*, *E*) were determined using 40–60 experimental reflections for each domain (the number of reflections taken into account depends on the domain considered). The calculated orientation matrices for all four domains are shown in Table 3. The average angular deviations calculated afterwards were less than 0.02° for all reflections.

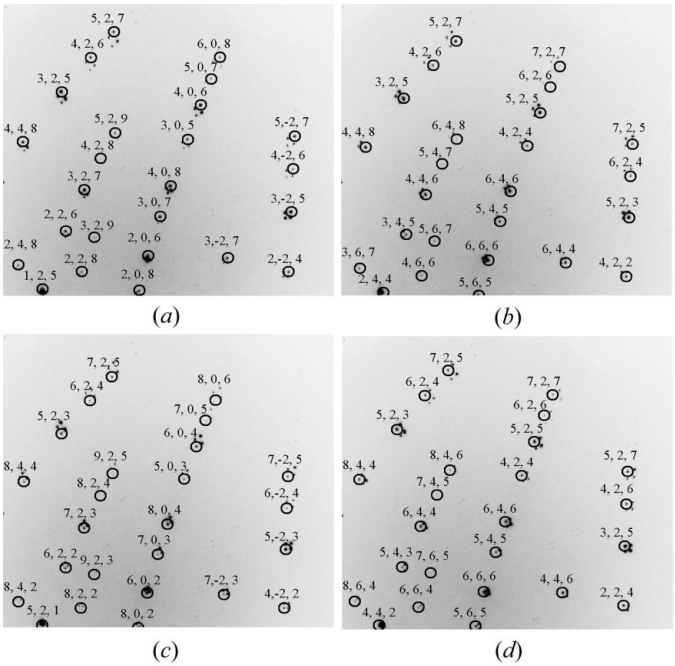

Figure 5
Indexing for domains *A* (*a*), *B* (*b*), *C* (*c*) and *E* (*d*) in an orthorhombic system with cell parameters a = 5.449, b = 7.794, c = 5.538 Å.

On the basis of equation (3) and using the experimental orientation matrices $\boldsymbol{M}_i$ for four domains, we calculated the relationship tensors $\boldsymbol{Tobs}_i$ as follows:

$$\boldsymbol{Tobs}_i = \boldsymbol{M}_i \times \boldsymbol{M}_A^{-1}, \qquad i = B, C, E. \tag{4}$$

The components of the tensors $\boldsymbol{Tobs}_i$ corresponding to the relationship for the three experimental domain pairs together with the theoretical relationship tensors $\boldsymbol{T}_t$ are listed in Table 1. From a comparison of the components of $\boldsymbol{T}_t$ and $\boldsymbol{Tobs}_i$, we can conclude that the observed domains *A*, *B*, *C* and *E* correspond to the D_1, D_6, D_2 and D_5 twin states, respectively. It can be seen that the domain labelled *A* is connected with domain *C* by the mirror plane $(10\bar{1})$, the domains *A* and *B* by mirror plane $(12\bar{1})$ or diad $[11\bar{1}]$, and domains *E* and *A* by mirror plane $(\bar{1}21)$ or diad $[\bar{1}11]$. Note that each possible domain pair D_1–D_i (i = 3 . . . 6) can be connected by two different domain walls and the components of tensors $\boldsymbol{T}_t$ have opposite signs and have close values for these cases (see Table 1). Different signs of the components of the tensor cannot be used to separate these kinds of domain walls because they also depend on the indexing process. As can be seen, the values of the components of the tensors $\boldsymbol{Tobs}_i$ differ in the third decimal, which does not allow the discernment of the difference between two possible domain walls (*W* mirror plane and *S* for *A*–*B* and *A*–*E* domain pairs). This is due to errors in the determination of the orientation matrices $\boldsymbol{M}_i$, which are larger than the difference in orientation of two allowed domains of the same state D_i in LSGM-05 crystal.

To separate these kinds of domain walls, we used a different method. Using the experimental orientation matrix $\boldsymbol{M}_A = \boldsymbol{M}_1$ for domain *A* and equation (3), we calculated the orientation matrices $\boldsymbol{M}_{ij}$ (i = 2 . . . 6, j = 1, 2) for all ten possible domains D_i. This allowed us to determine the coordinates of the Laue spots for all ten domains and their deviations relative to the Laue spots for D_1 (domain *A*) obtained by the method reported by Savytskii *et al.* (2003). Now we consider a single Laue spot, for example, 4,0,6 and its adjacent pixel region. Fig. 6 shows a comparison of the calculated and experimental spot shifts relative to the 4,0,6 reflection of D_1 (domain *A*) for allowed and observed domains. Clearly, the shifts associated with domains *B*, *C* and *E* are consistent with $(12\bar{1})$, $(10\bar{1})$ and $(\bar{1}21)$ domain walls, respectively. Note that the Miller indices for the reflections of different domains are different, for example, 5,2,5 for domains *B* and *E*, 6,0,4 for domain *C* . They correspond to ferroelastic shifts of domain *A* in domains *B*, *C* and *E*,

respectively, at which some planes turn into other ones. Furthermore, these indices agree with the pre-indexing of Laue patterns for the four observed domains *A*, *B*, *C* and *E* (Fig. 5).

In the above-mentioned theoretical and experimental analysis, we focused on one particular domain (D_1, domain *A*) and then analysed the data with respect to this domain. Such a choice is arbitrary and the results remain true for the other three possible cases: D_1 corresponding to domain *B*, *C* or *E*. Fig. 7 shows that we obtained similar results for the other cases: the Miller indexes of twin walls are the same if we take the corresponding domain *B*, *C* or *E* as the matrix. At the same time, experimental positions of all four domains are in very good agreement with the calculated ones for all four different choices of D_1. It shows that the domain structure is entirely composed of mutually permissible twin walls, and thus allows a stress-free intergrowth of all four domain states. Taking into consideration these foregoing results we can conclude that twin structure is formed by the intersection of domain walls $(12\bar{1})$ and $(10\bar{1})$ (see Fig. 8). The crystallographic plane $(12\bar{1})$ is the contact surface between domains *A* and *B*, and between domains *C* and *E*, whereas domains *A* and *C*, and *B* and *E* share a $(10\bar{1})$ wall. Its orientation changes by $\sim 90^\circ$ when crossing domain walls $(12\bar{1})$. Domains *A* and *E*, and *B* and *C* are only connected by crystallographic direction $[100]_p$ ($[101]$), which is common for the four domains. If we recognize domain *A* as D_1, then domain *B* corresponds to D_6, and domain *C* to D_2. Domains *B* and *E* are connected by mirror reflection with respect to $(10\bar{1})$, which exchanges lattice basic vectors **a** and **c** and preserves the orientation of vector **b** of the orthorhombic cell (Fig. 2, domain pair D_1–D_2). According to Fig. 2, the same space transformation of the lattice basic vectors of domain D_6 (domain *B*) (the exchange of **a** and **c** and

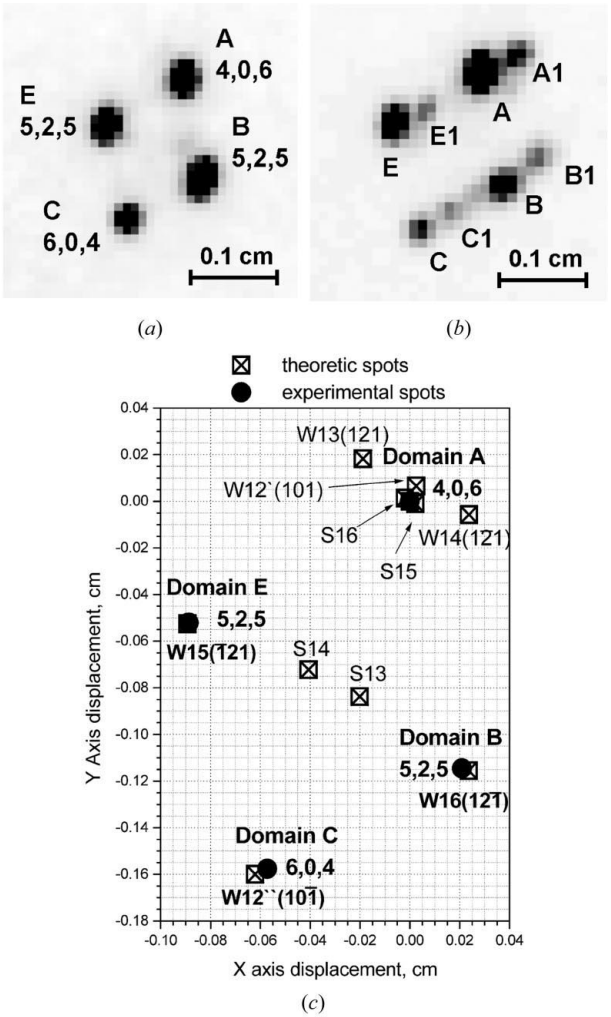

Figure 6
Enlarged experimental spots from (406), (525) and (604) planes (*a*) for four different (*A*, *B*, *C* and *E*) domains and (*b*) for the domains divided by a small-angle boundary. (*c*) Positional shifts of three domain (*B*, *C*, *E*) spots with respect to the matrix spot 4,0,6 (domain *A*) and calculated values for all possible twin laws in this crystal. A comparison of experimental (circles) and calculated (squares) spot shifts relative to the 406 reflection of domain *A* indicates that domain *A* is connected with the other three domains by mirror reflections relative to planes $(12\bar{1})$, $(10\bar{1})$ and $(\bar{1}21)$.

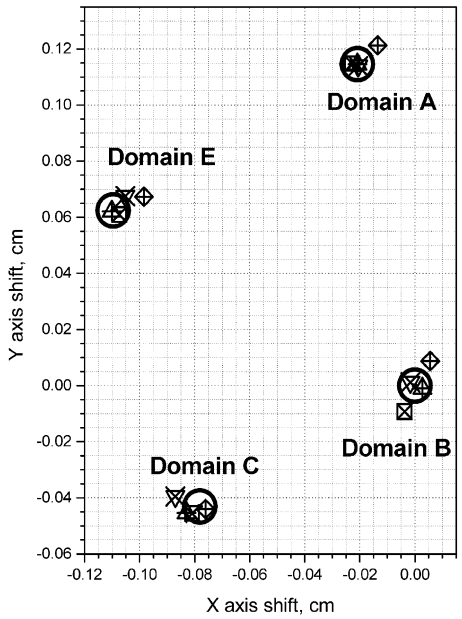

Figure 7
Experimental (circle) and calculated spot positions relative to the 525 reflection of domain *B* for the domain orientations with respect to domain *A* (up-triangle), *B* (square), *C* (rhomb) and *E* (down-triangle) as the matrix.

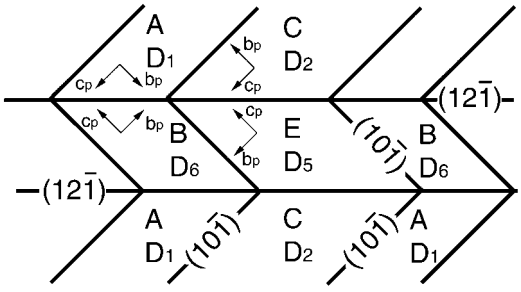

Figure 8
Schematic illustration of the twin structure formed by the intersection of domain walls $(12\bar{1})$ and $(10\bar{1})$.

the invariance of vector **b**) gives the cell orientation of state D_5 (domain E). From theoretical examination (Table 1), states D_5 and D_1 can be connected *via* mirror reflection of plane m_{yz} [$(\bar{1}21)$] or *via* rotation around the twofold axes 2_{yz} ([$\bar{1}11$]). Therefore, the wall is absent between domains A and E, but the orientation of both domains is the same as for mirror reflection by the $(\bar{1}21)$ plane. In other words, such a situation can be represented so that sequential reflection relative to the $(12\bar{1})$ and $(10\bar{1})$ planes is identical to mirror reflection by $(\bar{1}21)$ and in the perovskite setting it can be written schematically as

$$m_yF(m_{-yz}FD_1) = m_yFD_6 = D_5 = m_{yz}FD_1 = D_5$$
$$= m_{-yz}FD_2 = m_{-yz}F(m_yFD_1), \quad (5)$$

where the mF denotes mirror reflection of state D_i by the corresponding plane m.

Using a piezo stage, the sample surface has been scanned under the X-ray microbeam with 5 μm step size. In most scans the images were similar to the image shown in Fig. 6(*a*). Sometimes we observed more than four spots (as shown, for example, in Fig. 6*b*). Comparison of the experimental (Fig. 6*b*) and calculated spot shifts relative to the reflections of domains A, B, C and E indicates that domains $A1$, $B1$, $C1$ and $E1$ are not connected with the previous domains by any twin symmetry operation. Such parallel shifts are conditioned by a small-angle boundary, which divided two misorientated areas (0.2° in the case shown in Fig. 6*a*) with the same twinning structure (Fig. 8).

5. Conclusions

The X-ray microdiffraction Laue technique is well suited for the *in situ* study of twins, yielding information (misorientation between twins, twin laws, orientation of walls) on the sub-micrometre level both in small crystals and local areas of large samples. It can be used for non-destructive characterization of domain structure in materials with known crystal structure (crystal system and cell parameters). By comparing measurements of the mutual shift between twin spots with calculated values, it has been shown that the LSGM-05 crystal was mainly twinned relative to intersecting $\{12\bar{1}\}$ and $\{10\bar{1}\}$ mirror planes. The size of domains is less than 1 μm. It can be expected that the density of the domain walls (and types of walls) is the same (or bigger) in ceramic samples and has an influence on the ionic conductivity in LSGM compounds.

At the same time, the Laue technique gives the orientation of all observed domains, providing important information for the study of anisotropy of different properties in twinned crystals and films; for example, ionic conductivity and short vacancy ordering in the oxygen conductor (La,Sr)(Ga,Mg)O_{3-x}, charge ordering in (La,Ca)MnO_{3-x}, superconductivity in $YBa_2Cu_3O_{7-x}$, and so on.

The experiments were carried out at the Advanced Light Source, Berkeley, USA, supported by the Director, Office of Science, Office of Basic Energy Sciences, Materials Sciences Division, of the US Department of Energy under Contract No. DE-AC03-76SF00098 at Lawrence Berkeley National Laboratory. The authors acknowledge support from the Polish Committee for Scientific Research (Grant N 7T08A 00520) and the Ukrainian Ministry of Education and Science (Grant 'Ion'). DMT gratefully acknowledges financial support by the Deutscher Akademischer Austauschdienst (Leonhard–Euler program).

References

Aird, A. & Salje, E. K. H. (1998). *J. Phys. Condens. Matter*, **10**, L377–L380.
Aizu, K. (1970). *Phys. Rev. B*, **2**, 754–772.
Bartels, M., Hagen, V., Burianek, M., Getzlaff, M., Bismayer, U. & Wiesendanger, R. (2003). *J. Phys. Condens. Matter*, **15**, 957–962.
Chikaura, Y., Iida, S., Kawado, S., Mizuno, K., Kimura, S., Matsui, J., Umeno, M., Ozaki, T., Shimura, T., Suzuki, Y., Izumi, K., Kawasaki, K., Kajiwara, L. & Ishikawa, T. (2001). *J. Phys. D*, **34**, A158–A162.
Feng, M. & Goodenough, J. B. (1994). *Eur. J. Solid State Inorg. Chem.* **31**, 663–672.
Huang, X. R., Jiang, S. S., Liu, W. J., Wu, X. S., Feng, D., Wang, Z. G., Han, Y. & Wang, J. Y. (1996). *J. Appl. Cryst.* **29**, 371–377.
Ishihara, T., Matsuda, H. & Takita, Y. (1995). *Solid State Ion.* **79**, 147–151.
Janovec, V. (1972). *Czech. J. Phys. B*, **22**, 974–994.
Lee, W. T., Salje, E. K. H. & Bismayer, U. (2003). *Phase Transit.* **76**, 81–102.
Medrano, C., Schlenker, M., Baruchel, J., Espeso, J. & Miyamoto, Y. (1999). *Phys. Rev. B*, **59**, 1185–1195.
Putnis, A. & Salje, E. K. H. (1994). *Phase Transit.* **48**, 85–91.
Sapriel, J. (1975). *Phys. Rev. B*, **12**, 5128–5140.
Savytskii, D., Senyshyn, A., Matkovskii, A., Vasylechko, L., Wieteska, K., Wierzchowski, W., Lukasiewicz, T. & Bismayer, U. (2003). *Z. Kristallogr.* **218**, 17–25.
Tamura, N., Spolenak, R., Valek, B. C., Manceau, A. M., Chang, M., Celestre, R. S., MacDowell, A. A., Padmore, H. A. & Patel, J. R. (2002). *Rev. Sci. Instrum.* **73**, 1369–1372.
Tendeloo, G. van, Broddin, D., Zandbergen, H. W. & Amelinckx, S. (1990). *Physica C*, **167**, 627–639.
Vasylechko, L., Vashook, V., Savytskii, D., Senyshyn, A., Ullmann, H., Berkowski, M. & Matkovskii, A. (2003). *J. Solid State Chem.* **172**, 396–411.
Yao, G.-D., Dudley, M., Wang, Y., Liu, X. & Liebermann, R. C. (1991). *Mater. Sci. Eng. A*, **132**, 23–30.
Zhu, Y., Suenaga, M. & Moodenbaugh, A. R. (1990). *Philos. Mag. Lett.* **62**, 51–54.